

An $H\beta$ surge and X-ray jet – Magnetic properties and velocity patterns

J. Zhang^{1,2}, J. Wang^{1,2}, and Y. Liu¹

¹ Beijing Astronomical Observatory, Chinese Academy of Sciences, Beijing 100012, P.R. China
(zjun@ourstar.bao.ac.cn; wjx@ourstar.bao.ac.cn)

² National Astronomical Observatories, Chinese Academy of Sciences, Beijing 100012, P.R. China

Received 12 May 2000 / Accepted 19 July 2000

Abstract. We described simultaneous observations of a surge in $H\beta$ and an X-ray jet in NOAA 8100 on November 1, 1997. We found that the $H\beta$ surge was spatially coincident with the X-ray jet. They occurred at the site where the pre-existing magnetic flux was “cancelled” by a newly emerging flux of opposite polarity. At the base of the surge we identified surge-flaring in the $H\beta$ filtergrams, and both blueshifts and redshifts in the $H\beta$ Dopplergrams. The X-ray jet appeared about 2 hours after the first appearance of the surge. The surge consisted of two ejecting threads. Initially, these two components were twisted together, then became untwisted before the appearance of the X-ray jet. This example presents an alternative scenario of plasma ejection. The magnetic reconnection in the lower atmosphere, which was responsible for the $H\beta$ surge, created the twisted surge threads; the X-ray jet likely resulted from a fast reconnection in the upper atmosphere, which took place well after the $H\beta$ surge.

Key words: Sun: chromosphere – Sun: magnetic fields – Sun: X-rays, gamma rays

1. Introduction

$H\alpha$ surges have been studied for more than 50 years (see Roy 1973a, b). They are straight or slightly curved ejections that reach peak velocities of 50–200 km s⁻¹. They reach heights of up to 200,000 km and typically last 10–20 minutes. The surge material either fades or returns into the chromosphere along the trajectory of ascent (Svestka 1976; Tandberg-Hanssen 1977; Foukal 1990). At high spatial resolution, it is evident that the $H\alpha$ surges are highly filamentary in structure (Roy 1973a; Zirin 1988, pp. 296–301). On the other hand, X-ray jets were revealed by the Soft X-ray Telescope (SXT) of YOHKOH (Tsuneta et al. 1991). Their characteristics have been carefully described (Shibata et al. 1992a; Shibata et al. 1994; Schmieder et al. 1995). Of particular interest have been efforts to identify the relationship between cool plasma ejection, represented by $H\alpha$ or $H\beta$ surges, and hot plasma ejection, represented by brightening or

jets seen in EUV and X-ray. Rust et al. (1977) found that few $H\alpha$ surges were coincident with noticeable changes in X-ray emission. Schmieder et al. (1988) compared $H\alpha$ surge observations with relevant UV and X-ray data and supported the idea that $H\alpha$ surges are spatially correlated with UV and X-ray emissions. Shibata et al. (1992a) presented an example which showed that an X-ray jet is nearly co-spatial with an $H\alpha$ surge. However, Canfield et al. (1996) reported that X-ray jets are not co-spatial with $H\alpha$ surges, even though they are associated with each other. Recently, a similar result was obtained by Chae et al. (1999), who showed that the $H\alpha$ surges are not co-spatial with the EUV jets. In brief, most of the previous studies seem to support that $H\alpha$ surges are associated with EUV/X-ray brightening and jets, but the temporal and spatial relationship between them is still not clear.

There are many models devoted to the interpretation of solar dynamic phenomena such as surges and jets (see the detailed discussion by Schmieder et al. 1995, and Canfield et al. 1996). It is well accepted that surges are closely correlated with newly emerging flux in the periphery of sunspots or large-flux concentrations. They are manifestations of the magnetic reconnection between newly emerging and pre-existing flux. In a few careful studies (Schmieder et al. 1995; Yokoyama & Shibata, 1995; and Canfield et al. 1996), $H\alpha$ surges and X-ray jets are viewed as cool and hot components of plasma ejecta, respectively, and both hot and cool plasma are accelerated in a single magnetic reconnection. Since a surge is an outward ejection in the chromosphere, the reconnection site at the surge base could not be very high in the atmosphere, say, somewhere in the photosphere or lower chromosphere. Although the reconnection in the lower atmosphere is able to account for the cool plasma ejection, it seems to be difficult to interpret the creation of X-ray jets (the hot plasma ejection).

In this paper, we described in detail the interacting threads in an $H\beta$ surge and the subsequent X-ray jet, as well as the associated magnetic environment and evolution. This example shows that the $H\beta$ surge appears much earlier, caused by the magnetic reconnection in the lower atmosphere, while the X-ray jet appears well after, possibly caused by a fast reconnection in the upper atmosphere.

Send offprint requests to: J. Zhang

2. Instrumentation

The optical data for this paper include narrow band H β filtergrams and Dopplergrams, Fe λ 5324 vector magnetograms in the photosphere. They were obtained by the Solar Magnetic Field Telescope (SMFT), a magnetograph system (Ai & Hu 1986) installed at Huairou Solar Observing Station (HSOS) of the Beijing Astronomical Observatory. The SMFT consists of a 35-cm refractor with a vacuum tube, a birefringent filter, a CCD camera and an imaging processing system controlled by computer. The birefringent filter is tunable between two setups, working either at the photospheric line, FeI 5324 Å, with a 0.150 Å bandpass, or at the chromospheric H β line, with a 0.125 Å band pass.

A complete vector magnetogram is reconstructed from four narrow-band images of Stokes parameters transmitted by the birefringent filter. They are “ I ”, “ V ”, “ Q ”, “ U ”, respectively. Image V is the difference between the left and right circularly polarized images taken with the bandpass at 0.075 Å from the line center of Fe 5324 Å; Q and U are the differences between two orthogonal linearly polarized images for different azimuthal directions. When Q and U are taken, the filter bandpass is switched to the line center for achieving maximum sensitivity. I is always the “direct” intensity, derived from either the sum of two circularly polarized images for the line-of-sight field measurements, or the sum of two linearly polarized images for the transverse measurements. Both theoretical and empirical methods are used to calibrate the HSOS vector magnetogram. The relationship between the magnetic field specified by the atmospheric model and the fractional intensities of Stokes parameters is established as

$$B_{\parallel} = C_{\parallel} \frac{V}{I} \quad (1)$$

$$B_{\perp} = C_{\perp} \left(\frac{Q^2}{I^2} + \frac{U^2}{I^2} \right)^{1/4} \quad (2)$$

where C_{\parallel} ($= 10.00 \times 10^3$ G) and C_{\perp} ($= 9.73 \times 10^3$ G) are calibration coefficients for line-of-sight and transverse magnetograms (Wang et al. 1996), respectively. Observations presented in this paper were taken at good seeing. For the line-of-sight magnetogram with 256 integrated image pairs, used for this work, the noise level is about 15 G. For the transverse field measurements, the noise level is estimated from the standard deviation of the transverse field in weak field areas. We find the noise is about 100 G.

The H β Dopplergrams may contain many components such as solar rotation, steady flows, oscillation, convection, and evolutionary features. In this work, we are mostly interested in the evolutionary component. The solar rotation and steady flow are eliminated by subtracting a smooth background field, while the oscillation and convection are much smaller than the evolutionary component in magnitude. The spatial resolution for both magnetograms and Dopplergrams is 2 ~ 3 arcsec. Lacking full spectral information and adequate spatial resolution, the Doppler signals from filter-based observations may be considered as spectral and spatial averages of the true features.

The pixel size of the CCD for HSOS data is 0.''613 and 0.''425 in the east-west and south-north directions, at the time of

this observation. To acquire 256 integrated image pairs takes approximately 41 seconds for the SMFT system. High-frequency distortion by seeing practically specifies the real angular resolution, which is approximately 2'' ~ 3'' for this set of magnetograms. This would certainly not enable one to resolve the intrinsic magnetic structures in active regions. In this case, the line-of-sight magnetogram measures the flux density in the resolved area.

The Solar and Heliospheric Observatory (SOHO), a joint European Space Agency (ESA) and National Aeronautics and Space Administration (NASA) effort, was launched late in 1995 and has provided unprecedented observations of the Sun and heliosphere. In this paper, we present observations made by two of the instruments on SOHO, the Michelson Doppler Imager instrument (MDI) and the Extreme Ultraviolet Imaging Telescope (EIT). A detailed description of these instruments is provided by Scherrer et al. (1995) and Delaboudinière et al. (1995). The YOHKOH Soft X-ray Telescope (SXT) (Tsuneta et al. 1991) observes the Sun in the wavelength range 3–50 Å with an instrumental pixel size of 2''.5. All SXT images in this paper were taken through the thin aluminum (A1.1) filter, at various levels of resolution (full, half, quarter) corresponding approximately to 2''.5, 5'', or 10'' pixel size, respectively.

To compare data from several instruments, data alignment is extremely important. For this study, the alignment is relatively easy, as HSOS H α filtergrams, SOHO/EIT, MDI and YOHKOH soft X-ray images were all full disk data. Alignment among these images was easily done by limb fitting. The HSOS H β images then are aligned with the HSOS full disk H α images, and the HSOS magnetograms are aligned with H β images, as their field-of-view are the same. The final coalignment error is estimated to be about 5'' on the basis of the uncertainty in orientations.

3. Observational properties

The observations we analyzed were obtained by HSOS, YOHKOH/SXT, SOHO/EIT and MDI on November 1, 1997. The plasma ejection, manifested as an H β surge, EUV and X-ray jet, was observed at the boundary of the main sunspot of NOAA 8100 at position S18E10. Fig. 1 shows the general appearance of the H β surge. In the figure, Panel ‘A’ is a line-of-sight magnetogram at 03:16 UT, superposed by a surge as a contour at 03:42 UT. In the magnetogram, the brighter patches are the positive polarity fields, and the darker patches, the negative ones. Panel ‘B’ is a portion of the YOHKOH SXT image at 04:15 UT; the X-ray jet is indicated by an arrow. The white patch underneath the jet is an X-ray bright point. Panel ‘C’ is an H β filtergram at 03:42 UT taken at -0.24 Å from the line center, the brighter patch under the base of the surge is a surge-flare. Panel ‘D’ is an H β Dopplergram at 02:37 UT, where the brighter patches are downward motion, and darker ones, upward motion. This figure shows the appearance of the plasma ejection at different wavelengths and in the different layers of the Sun accordingly (e.g., H β in the lower chromosphere, X-ray in the corona at temperature above 2.5 MK).

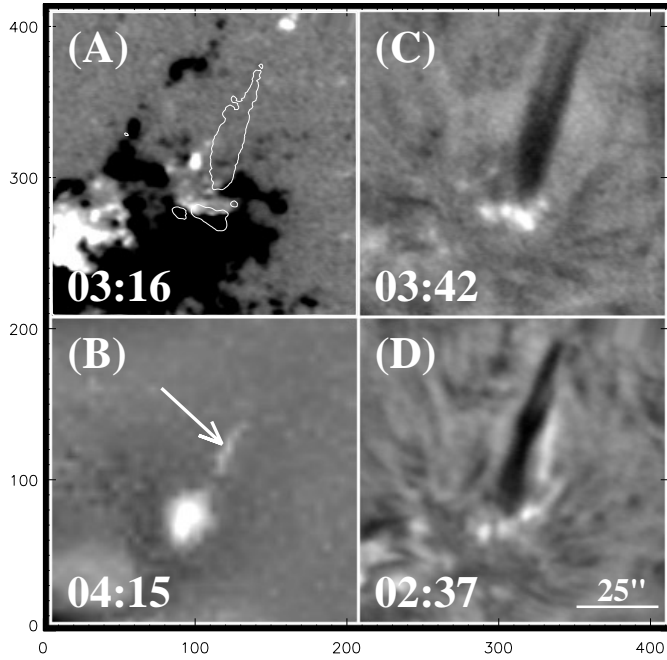


Fig. 1a–d. General appearance of the surge. **a** line-of-sight magnetogram at 03:16 UT, superposed by the surge as contour at 03:42 UT; **b**: a portion of the *Yohkoh* SXT image of 04:15 UT, the arrow shows an X-ray jet; **c**: an H β filtergram at 03:42 UT taken at -0.24 \AA from the line center; **d**: an H β Dopplergram at 02:37 UT.

3.1. Morphology and velocity

Fig. 2 is time sequence of H β filtergrams (the first and third columns) and Dopplergrams (the second and fourth columns). The surge appeared before 02:21 UT (there were no H β data at the early phase of the surge), and lasted two and a half hours. It consisted of several components. At 02:29 UT, two threads (shown by two arrows) had bright points at their bases, the third one on the right was smaller than the other two and had no bright point at its base. The two larger threads twisted together at 02:37 UT, which could be seen more clearly in H β Dopplergrams. It was clearly seen that the two twisted components were blue shifted, and a red shifted component (see the arrow at 02:37 UT) appeared on the right at the same time. This indicated that while the major part of the material of the surge moved upward, a fraction of the material moved downward. At 03:23 UT, the two blue-shift components merged at their tops, then at 03:39 UT, the once amalgamated tops of the two threads separated. We suggest that this phenomenon presents the untwisting process. During the decay phase of the H β surge, more fractions of threads became red-shift (denoted by two arrows at 03:56 and 04:38 UT), and an X-ray jet appeared (see following). In order to demonstrate the velocity patterns of the H β surge more clearly, we present in Fig. 3 four selected Dopplergrams at critical times when key evolutions were seen. The two blue shifted components twist (at 02:37 UT), untwist (at 03:23, 03:39 UT) and rotate (03:56 UT).

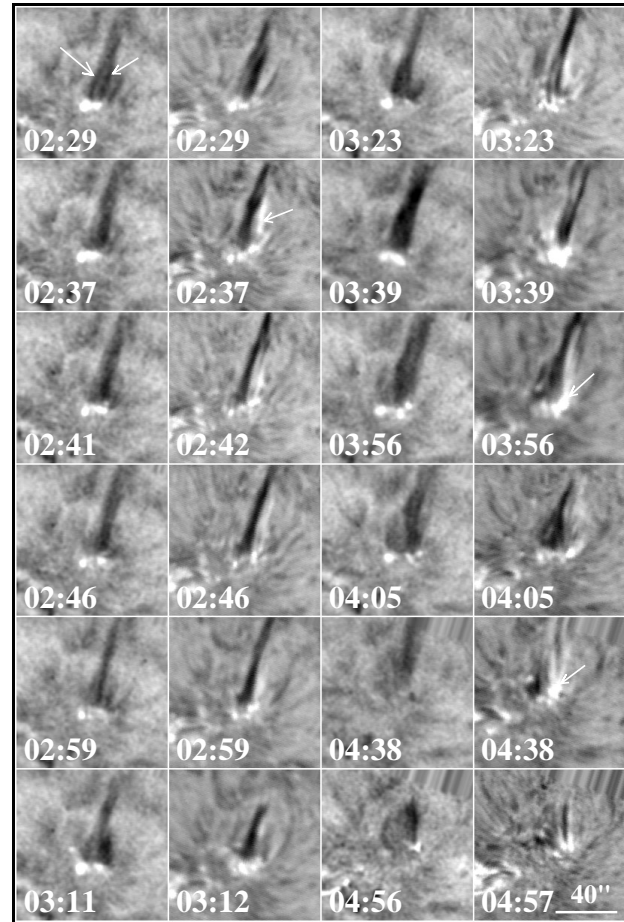


Fig. 2. Comparison of time sequences of H β filtergrams (the first and third columns) and Dopplergrams (the second and fourth columns). The two arrows at 02:29 UT show the two main components of the H β surge. Arrows at 02:37, 03:56, and 04:38 UT in Dopplergrams indicate red-shift components of the surge.

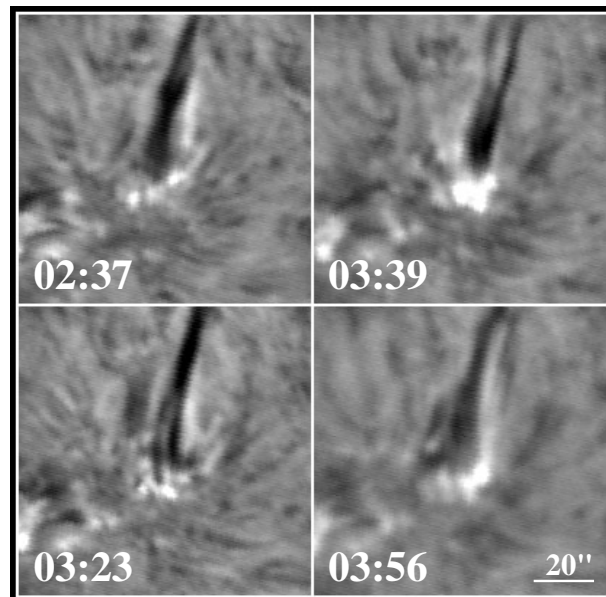


Fig. 3. Velocity patterns seen in H β Dopplergrams.

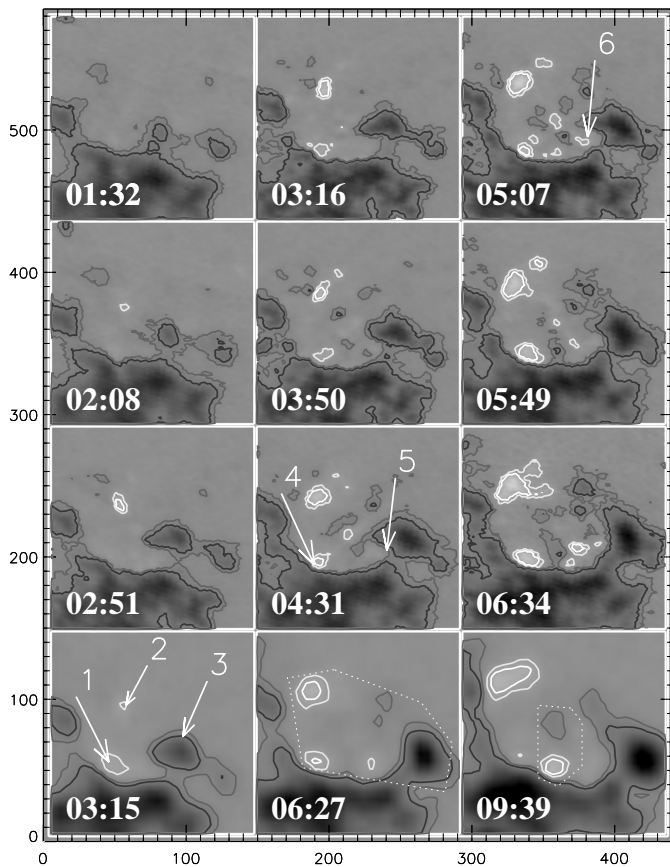


Fig. 4. Time sequences of line-of-sight magnetograms showing the magnetic fields evolution on the base of the $H\beta$ surge, superposed by iso-gauss contours with levels ± 50 and 100 G. The positive (negative) polarity fields are represented by brighter (darker) color in the grey scale maps and white (dark) contours in the iso-gauss drawings. The upper three rows show the magnetograms from HSOS, and the lowest row from SOHO/MDI. The close curves at 06:27 and 09:39 UT present two emerging magnetic bipoles which associated with the $H\beta$ surge. Three arrows at 03:15 UT show three magnetic flux patches of the emerging magnetic bipole closed by the curve 06:27 UT. Two arrows at 04:31 UT mark the foot points of the $H\beta$ surge. Arrow at 05:07 UT shows the magnetic field at a surge foot. The field of view is about 50 by 50 arcsec.

3.2. Magnetic fields

In Fig. 4 we present the time sequence of line-of-sight magnetograms showing the magnetic field evolution on the base of the $H\beta$ surge. Iso-gauss contours with levels ± 50 and 100 G are superposed on the grey-scale maps to demonstrate the field evolution more clearly. The upper three rows are the magnetograms from HSOS, and the lowest row is taken from SOHO/MDI full disk magnetograms. We find that the magnetograms from HSOS and SOHO/MDI are consistent in morphology, but the spatial resolution of the HSOS magnetograms is higher than that of SOHO/MDI. The positive (negative) polarity fields are represented by brighter (darker) color in the grey scale maps and white (dark) contours in the iso-gauss drawings. The close curves at 06:27 and 09:39 UT represent two emerging magnetic

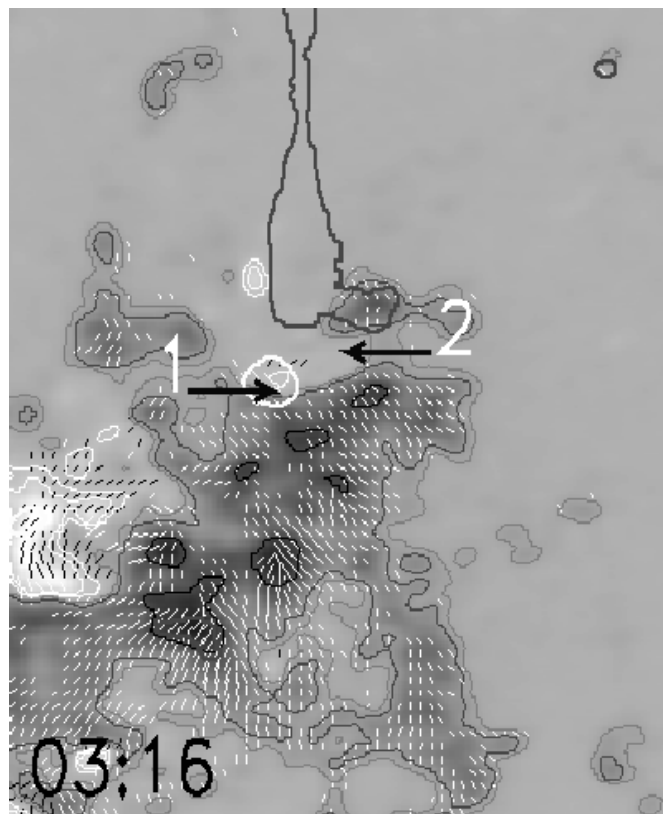


Fig. 5. A set of vector magnetogram taken near 03:16 UT, superposed by the surge (surge flaring) as dark (white) thick contour at 03:23 UT. The line-of-sight components are presented by grey scale map and by iso-gauss contours with levels ± 50 , 100 and 400 G; the transverse components are presented by short line segments with length proportional to the field strength and alignment parallel to the field direction. Two arrows show the foot points of the $H\beta$ surge. The field of view is about 105 by 120 arcsec.

bipoles respectively. These bipoles are associated with the $H\beta$ surge. Usually, a new emerging magnetic bipole manifests itself in one of two ways. One way is the appearance of arch filament systems in $H\alpha$ and/or $H\beta$ filtergrams; the second is co-temporal growing and separating of opposite polarity flux in line-of-sight magnetograms. In this figure, we determine the emerging bipoles by the second way from a continuous 30 hour time-sequence of SOHO/MDI magnetograms. Three arrows at 03:15 UT show magnetic flux patches of an emerging magnetic bipole outlined by the curve at 06:27 UT. The positive magnetic flux (shown by arrow ‘1’) was cancelled by a pre-existing large-scale negative flux during its emergence, and finally disappeared near 09:39 UT. The other two flux patches grew continuously since they did not encountered a flux of opposite polarity. Two arrows at 04:31 UT show the foot points of the $H\beta$ surge. We can see clearly the evolution of magnetic fields on the base of the $H\beta$ surge. One end (shown by arrow ‘4’) of the $H\beta$ surge is rooted at the cancellation site mentioned above. Arrow ‘6’ at 05:07 UT shows a positive flux patch which might have already cancelled with the nearby negative polarity field before appearing in the photosphere. This cancellation seems to cor-

respond to another component of the $H\beta$ surge indicated by arrow ‘5’. It is shown by the time-lapse $H\beta$ filtergrams that the $H\beta$ surge appeared before 02:21 UT. However, the time sequence of HSOS/MDI magnetograms demonstrated that the positive flux of the new emerging bipole had not appeared in the photosphere until 03:16 UT, which was about one hour later than that of the first appearance of the $H\beta$ surge. Surge appears at the early stage of flux emergence, and is often (Kurokawa & Kawai, 1993) considered the first signature of an emerging flux region. From the spatial relationship we believe that the $H\beta$ surge analysed is intrinsically correlated with the new emerging flux outlined at 06:27 UT. This surge presents a nice example that surge appears before the new emerging flux broken up in the photosphere. If we accept the idea that surge results from magnetic reconnection between new and pre-existing flux, then in this example the reconnection must have taken place below the photosphere. In a sense, we could conclude the $H\beta$ surge studied manifested an interaction, which took place at quite low atmosphere, between the newly emerged flux and the pre-existed large-scale magnetic fields of opposite polarity of AR 8100. Fig. 5 shows a vector magnetogram taken near 03:16 UT, superposed by the surge (surge-flaring) as dark (white) thick contour at 03:23 UT. The line-of-sight components are presented by both grey scale map and iso-gauss contours with levels ± 50 , 100 and 400G; the transverse components are presented by short line segments with length proportional to the field strength and alignment parallel to the field direction. Two arrows show the foot points of the $H\beta$ surge.

3.3. EUV and X-ray jet

Among various newly discovered dynamic phenomena, one of the most interesting findings are EUV and X-ray jets (Schmahl, 1981; Chae et al. 1999; Shibata et al. 1992b; Strong et al. 1992). According to Shibata et al. (1992b), X-ray jets are transitory X-ray emission enhancements with an apparent collimated motion. Chae et al. (1999) reported that EUV jets occur repeatedly at the regions where pre-existing magnetic flux is ‘cancelled’ by newly emerging flux of opposite polarity. Fig. 6 shows SOHO/EIT 195 Å running difference images from 01:43 to 04:33 UT and an MDI magnetogram (middle-left panel). Arrow ‘1’ at 04:51 UT showed the interface of newly emerging positive flux and negative sunspots. The interaction of these magnetic fields triggered an EUV bright point and EUV jet, which were denoted by two arrows ‘2’ and ‘3’ at 04:16 UT EIT image. Comparing $H\beta$ filtergrams with EUV images, We find that the $H\beta$ surge is spatially coincident with the EUV jet, although the EUV jet appeared later than the $H\beta$ surge. From the EIT movie, we find that the material of the EUV jet moves along a large-scale loop. Fig. 7 is time sequences of SXT images showing an X-ray bright point and jet appeared at 04:15:05 UT. A SOHO/MDI magnetogram at 04:51 UT was presented to show the magnetic fields configuration associated with the X-ray bright point (arrow ‘2’) and jet. Mandrini et al. (1996) found evidence showing that X-ray bright point brightenings were due to magnetic reconnection between a new bipole and pre-existing plage fields; Schmieder et

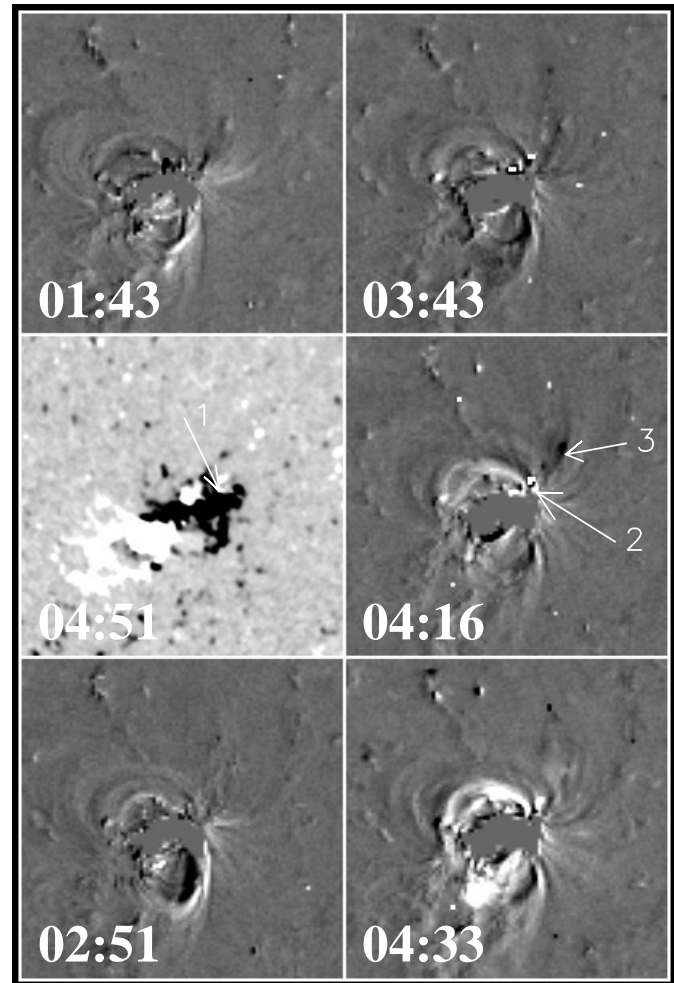


Fig. 6. SOHO/EIT running difference images and an MDI magnetogram (middle-left panel). The arrow at 04:51 UT showed the interface of two opposite polarity magnetic fields. The interaction of these magnetic fields triggered an EUV bright point and EUV jet, which were denoted by two arrows at EIT image at 04:16 UT. The field of view is about 500 by 500 arcsec.

al. (1997) presented that X-ray loops (bright points) appeared at the location of a emerging flux. From the time series of SXT images studied, we found that there were two X-ray bright points. The first appeared near 03:38 UT, meanwhile the twisted components of the $H\beta$ surge untwisted. The second occurred at the same site as the first, where sunspot negative flux was “cancelled” (shown by arrow ‘1’ at 04:51 UT) by a positive flux of the new emerging flux region described in Sect. 3.2. Near 04:15 UT, the decay phase of the $H\beta$ surge, an X-ray jet took place in the company of the second X-ray bright point. Unfortunately, there were no $H\beta$ data at the onset phase of the X-ray jet, we did not know the evolution of the $H\beta$ surge at the time of the X-ray jet appearance. We suggest that the two X-ray bright points were a consequence of an explosive reconnection in the corona during the continuous flux cancellation (Nolte et al. 1979). The $H\beta$ surge and X-ray jet may well represent a scenario of two-step reconnection, proposed first by Wang & Shi (1993) for flare

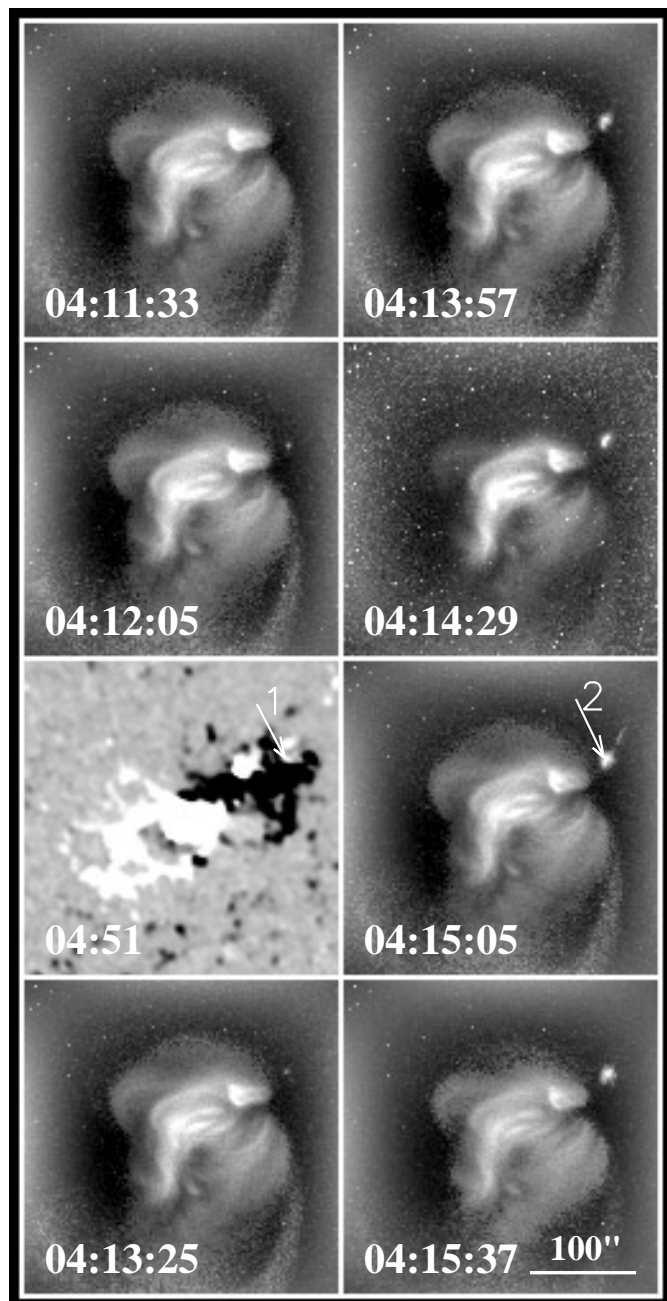


Fig. 7. Time sequences of SXT images showing the X-ray bright point and X-ray jet that appeared at 04:15:05 UT. A SOHO/MDI magnetogram at 04:51 UT is presented to show the magnetic fields configuration associated with an X-ray bright point and jet. Arrow '1' shows a magnetic cancellation site which responded to the X-ray bright point (arrow '2').

observations, and confirmed by Chae et al. (1999) for EUV explosive events. The first-step reconnection takes place in the photosphere, or lower atmosphere. It is slow but continuous since the conductivity in the photosphere is much lower than that of the fully-ionized plasma in the upper chromosphere and corona. This slow reconnection manifests as flux cancellation observed in the photospheric magnetograms (Livi et al. 1985;

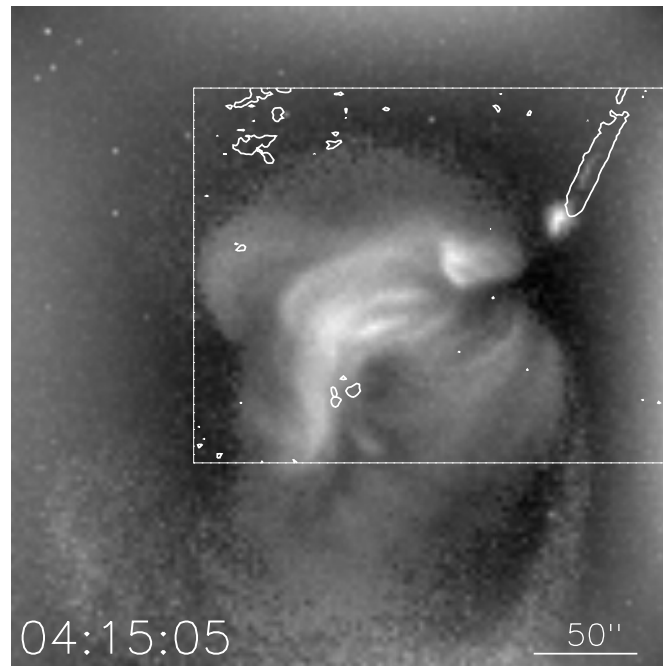


Fig. 8. The SXT image taken from 04:15:05 UT, superposed on the $H\beta$ surge at 03:42 UT.

Martin et al. 1985). The reconnection in the lower atmosphere may convert the magnetic energy into heat and kinetic energy; while, at the same time, it can transport the magnetic energy and complexity into the rather large-scale magnetic structure higher in the corona. The second-step reconnection can only take place when some critical status is achieved in the large-scale magnetic structure higher in the corona. This reconnection is explosive in nature, which is directly responsible for the energy released in the transient solar activities. Fig. 8 is an X-ray image at 04:15:05 UT superposed by the contours of $H\beta$ filtergram at 03:42 UT. Despite the low spatial resolution of the X-ray image, it is clear that the $H\beta$ surge and X-ray jet are co-spatial, although the length of the $H\beta$ surge appears longer than that of the X-ray jet.

4. Conclusions and discussions

In this paper we have presented an example of a hot plasma jet, seen in YOHKOH SXT and SOHO EIT images, that is co-spatial with cool plasma ejection, observed as an $H\beta$ surge. However, the X-ray jet took place only in the late stage of the $H\beta$ surge. As shown by previous studies, the surge appeared at the boundary between newly emerging magnetic flux, e.g. parasite polarity, and the pre-existing main flux of an active region. Evidence is first shown by this study that with the interaction of parasite and main magnetic flux, threads of the surge become twisted, and present complicated Doppler patterns. The X-ray jet appears right after the $H\beta$ surge, became untwisted, and downstreaming appeared at the surge base.

For the event studied we would suggest that the $H\beta$ surge was caused by the slow reconnection in the lower atmosphere at the very early stage of a vigorous EFR which was fully de-

veloped on November 4. It was suggested that surges are due to magnetic reconnection between a twisted cool loop and open field lines (Schmieder et al. 1995). The twisting of surge threads is indicative that the large-scale loops in the corona had been charged, i.e. became current-carrying. In the other words, free magnetic energy and magnetic complexity had been accumulated in the surge threads. The fast reconnection then took place and manifested as an X-ray jet. Both the transient X-ray brightening and the downstreaming which was observed in the later phase of the H β surge might signal the fast reconnection in the higher atmosphere. This two-step reconnection process seems to be common in transient solar activities. Chae et al. (1999) found indications of the two-step process in transition region explosive events. Further observational studies and theoretical approaches are crucially required to confirm, improve, or disprove the two-step reconnection scenario of solar transient events.

Acknowledgements. This work was supported by the Major Project 19791090, funded by the National Natural Science Foundation of China (NSFC). The authors are indebted to the Huairou staff for obtaining good observations. We are grateful to all members of YOHKOH team for providing the wonderful Yohkoh data. We also would like to thank the SOHO MDI and EIT teams for observing the data. SOHO is a project of international cooperation between ESA and NASA.

References

- Ai G., Hu Y., 1986, *Publ. Beijing Astron. Obs.* 8, 1
 Canfield R.C., Peadar K.P., Leka K.D., et al., 1996, *ApJ* 464, 1016
 Chae J., Qiu J., Wang H., Goode P.R., 1999, *ApJ* 513, L75
 Delaboudinière J-P., Artzner G.E., Brunaud J., et al., 1995, *Solar Phys.* 162, 291
 Foukal P., 1990, In: *Solar Astrophysics*. Wiley, New York, p. 354
 Kurokawa H., Kawai G., 1993, In: Zirin H., Wand H. (eds.) *ASP Conf. Ser. 46, The Magnetic and Velocity Fields of Solar Active Regions*. ASP, San Francisco, p. 507
 Livi S.H.B., Wang J., Martin S.F., 1985, *Aust. J. Phys.* 38, 855
 Mandrini C.H., Démoulin P., van Driel-Gesztelyi L., et al., 1996, *Solar Phys.* 168, 115
 Martin S.F., Livi S.H.B., Wang J., 1985, *Aust. J. Phys.* 38, 929
 Nolte J.T., Solodyna C.V., Gerassimenko M., 1979, *Solar Phys.* 63, 113
 Roy J.-R., 1973a, *Solar Phys.* 28, 95
 Roy J.-R., 1973b, *Solar Phys.* 32, 139
 Rust D.M., Webb D.F., MacCombie W., 1977, *Solar Phys.* 54, 53
 Scherrer P.H., Bogart R.S., Bush R.I., et al., 1995, *Solar Phys.* 162, 129
 Schmahl E.J., 1981, *Solar Phys.* 69, 135
 Schmieder B., Simnett G.M., Tandberg-Hanssen E., Mein P., 1988, *A&A* 201, 327
 Schmieder B., Shibata K., van Driel-Gesztelyi L., Freeland S., 1995, *Solar Phys.* 156, 245
 Schmieder B., Aulanier G., Démoulin P., et al., 1997, *A&A* 325, 1213
 Shibata K., Ishido Y., Acton L.W., et al., 1992a, *PASJ* 44, L173
 Shibata K., Nozawa S., Matsumoto R., 1992b, *PASJ* 44, 265
 Shibata K., Yokoyama T., Shimojo, M., 1994, In: Enome S., Hirayama T. (eds.) *New Look at the Sun with Emphasis on Advanced Observations of Coronal Dynamics and Flares*. NRO Rep. 360, p. 75
 Strong K.T., Harvey K., Hirayama T., et al., 1992, *PASJ* 44, L161
 Svestka Z., 1976, *Solar Flares*. Reidel, Dordrecht
 Tandberg-Hanssen E., 1977, In: Bruzek A., Durrant C.J. (eds.) *Illustrated Glossary for Solar and Solar-terrestrial Physics*. Reidel, Dordrecht, p. 106
 Tsuneta S., Acton L.W., Bruner M., et al., 1991, *Solar Phys.* 136, 37
 Wang J., Shi Z., 1993, *Solar Phys.* 143, 119
 Wang J., Shi Z., Wang H., Lü Y., 1996, *ApJ* 456, 861
 Yokoyama T., Shibata K., 1995, *Nat* 375, 42
 Zirin H., 1988, *Astrophysics of the Sun*. Cambridge Univ. Press, Cambridge